ACS Catalysis

Research Article

pubs.acs.org/acscatalysis

# High-Yield Hydrogen Production from Aqueous Phase Reforming over Single-Walled Carbon Nanotube Supported Catalysts

Xiaoming Wang,*[,†] Nan Li,[‡] Zhiteng Zhang, Chuan Wang,[§] Lisa D. Pfefferle, and Gary L. Haller*

Department of Chemical and Environmental Engineering, Yale University, 9 Hillhouse Avenue, New Haven, Connecticut 06520, United States

Supporting Information

**ABSTRACT:** Pt and Pt−Co bimetallic catalysts supported on single-walled carbon nanotubes (SWNTs) were synthesized by a wet reduction−decoration method and tested for catalytic activity of aqueous phase reforming of ethylene glycol. The Pt decorated on SWNT achieves a catalyst mass time hydrogen yield of 890 micromole gcat$^{-1}$ min$^{-1}$, which is higher than the reported results for Pt−alumina catalyst. Experiments also show that this catalyst has better activity than Pt supported on activated carbon with a similar surface area, showing the advantage of SWNTs as a catalyst support. Factors affecting the aqueous phase reforming activity, such as temperature, pressure, WHSV, catalyst particle size, etc., were investigated. We have also explored Pt−Co bimetallic catalysts by combining the structural characterization results with the reactivity results and revealed that bimetallic catalysts may promote the catalyst performance in two different ways: either via the formation of Pt−Co alloy phase or via the synergistic catalytic activities of individual Pt and Co particles. The Pt−Co−SWNT catalyst achieved a hydrogen production activity as high as 4.6 mmol gcat$^{-1}$ min$^{-1}$.

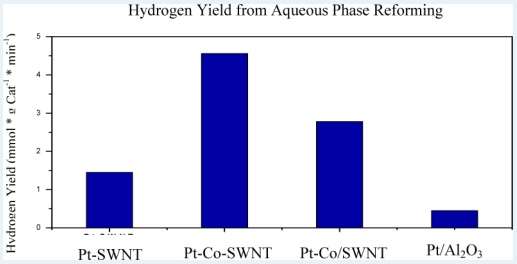


**KEYWORDS:** *aqueous phase reforming, bimetallic catalyst, hydrogen energy, single-walled carbon nanotubes, platinum, cobalt, biofuel, EXAFS*

## INTRODUCTION

Environmental crises that are a result of fossil fuel consumption, as well as the diminishing petroleum resources, have prompted our society to consider alternative fuels. Fuels developed from biomass have drawn much attention since they are sustainable and $CO_2$-neutral. Hydrogen, among all the alternative fuels, has the advantage that it can be derived from diverse domestic resources, is $CO_2$-neutral if derived from biological resources, and also can serve all sectors of the economy.[1] Therefore, generating hydrogen from biomass can be one contribution to resolving our energy problem. Aqueous phase reforming (APR), developed by Dumesic et al. in 2002, has been proposed as an attractive new route for the conversion of biomass-derived feedstocks.[2−8] Both we[9−11] and others[12,13] have demonstrated that carbon would be a good catalyst support for APR reaction because of its high hydrothermal stability. We have studied both single-walled carbon nanotube (SWNT)- and multiwalled carbon nanotube (MWNT)-supported catalysts for APR, and both Pt monometallic catalyst and Pt−Co bimetallic catalysts have been studied.[9−11] In this work, a high surface area SWNT synthesized in our laboratory was used as a catalyst support for APR. Both Pt monometallic catalysts and Pt−Co bimetallic catalysts have been prepared on SWNT supports, and their activities and selectivities for APR were explored. We have also compared the APR activities on supported Pt catalysts using different kinds of carbon supports.

Bimetallic catalysts are another topic that will be explored in detail in this work. Early work by Sinfelt and co-workers has demonstrated that by forming an alloy phase, bimetallic catalysts may show much higher performance than either component of the alloy, and this result may be attributed to the change of electronic structure of the metal upon alloy formation.[14] In recent years, there has been renewed interest in base metal addition to a precious metal catalyst, with the aim of reducing the use of precious metal in the catalyst. Considerable work has been performed on fuel cell catalysts because precious metals, especially Pt, are heavily used in fuel cells.[15−20] This work has been extended to reforming catalysts for both catalytic reforming[21−23] and APR.[8] In this article, SWNT-supported Pt−Co bimetallic catalysts will also be explored and tested in APR. The interaction between Pt and Co will be described in detail and will be correlated with the catalytic activity and selectivity results to obtain a structure−activity relationship in the SWNT-supported bimetallic catalysts.

## EXPERIMENTAL SECTION

**Catalyst Preparation.** The majority of the SWNT material used in this study was synthesized in our laboratory and is denoted ySWNT. Some SWNT material used in this study was purchased from Cheaptubes Inc. and is denoted cSWNT for reference purposes.

Received: December 22, 2011
Revised: June 6, 2012
Published: June 7, 2012

  

Table 1. Aqueous Phase Reforming Activities of Pt Monometallic Catalysts Supported on Different Carbon Support

| catalyst | prereduction | catalyst mass time yield[a] | Pt mass time yield[b] | % conversion[c] | % hydrogen selectivity[d] | % alkane selectivity[e] | % Pt loading[f] |
|---|---|---|---|---|---|---|---|
| Pt-ySWNT-EG | no | 1.45 | 21 | 13.3 | 93 | 8.1 | 6.9 |
| Pt-ySWNT-EG | yes | 0.89 | 13 | 8.3 | 94 | 10.0 | 6.9 |
| Pt-cSWNT-EG[g] | no | 0.51 | 6.5 | 4.5 | 92 | 12.6 | 7.8 |
| Pt-AC | no | 0.79 | 8.7 | 14.3 | ~100 | 11.2 | 9.1 |
| $Pt/Al_2O_3$[h] | yes | 0.45 | 15 | 5.4 | 87 | 1.2 | |

[a]Measured by millimoles hydrogen per gram catalyst per minute. [b]Measured by millimoles hydrogen per gram platinum in the catalyst per minute. [c]Evaluated by $CO_2$ production with respect to the ethylene glycol feed. [d]Calculated as (molecules $H_2$ produced/C atoms in gas phase)(2/5). [e]Calculated as (C atoms in gaseous alkanes)/(total C atoms in gas-phase product). [f]Calculated from the edge jump of XAS. [g]Data from ref 9. [h]Reference data from ref 8.

The synthesis of ySWNT is from a catalytic CO disproportionation reaction, in which CO disproportionates into SWNTs and $CO_2$, catalyzed by a Co-MCM-41 catalyst. The Co-MCM-41 catalyst was prereduced at 750 °C at ambient pressure before the SWNT synthesis, and the CO disproportionation was carried out at 750 °C and 80 psig. The details of the ySWNT synthesis were reported elsewhere.[24,25] The as-synthesized ySWNT was first treated in NaOH in ethanol solution to remove the MCM-41 template and then refluxed in concentrated HCl solution to remove the exposed Co particles. Then the sample was oxidized in air to remove amorphous carbon (the product of this step is denoted Co-ySWNT and also is used as a catalyst in this research) and to expose Co particles covered by carbon, followed by another HCl treatment to remove the Co particles that had been covered by carbon. The details of the purification process, which provides high-purity SWNTs, is also published elsewhere.[26]

Catalysts were prepared by two methods: impregnation and solution reduction. For catalysts prepared by impregnation, SWNTs were impregnated with an aqueous solution of tetra-amine platinum(II) nitrate (from Sigma-Aldrich) dropwise until incipient wetness. The concentration of the tetra-amine platinum(II) nitrate was adjusted according to the pore volume of the SWNTs to guarantee 8 wt % Pt loading. The catalysts prepared after incipient wetness impregnation were then dried overnight at 60 °C.

To prepare Pt−Co bimetallic catalysts via impregnation, the monometallic Pt/ySWNT catalysts were then impregnated with a cobalt(II) nitrate (from Sigma-Aldrich) solution until incipient wetness. The concentration of the cobalt solution was adjusted according to the pore volume of the support to guarantee 1:1 weight ratio between Pt and Co (i.e., 1:3.31 atomic ratio between Pt and Co). The nominal metal loading was also confirmed by the edge jump of X-ray absorption.[27] The catalyst obtained was denoted as Pt−Co/ySWNT.

The solution reduction method used to prepare both monometallic and bimetallic catalysts were prepared according to the method presented by Lordi et al.[28] The SWNTs were treated in 2.6 M nitric acid at 70 °C for 8 h, filtered, and dried overnight at 60 °C. The oxidized SWNTs were refluxed with $K_2PtCl_4$ (from Sigma-Aldrich) in aqueous ethylene glycol solution for 8 h in a recipe of 0.15 mg of $K_2PtCl_4$, 1.2 mL of ethylene glycol, and 0.8 mL of water for 1 mg of SWNTs, then filtered and dried. These products are denoted as Pt-ySWNT-EG and Pt-cSWNT-EG, respectively, and were used as a catalyst for APR. Co-ySWNT was also treated via the same process and labeled Pt−Co-ySWNT-EG. On the other hand, cobalt nitrate solution was impregnated onto Pt-ySWNT-EG by incipient wetness impregnation, and the catalyst obtained was denoted as Pt-ySWNT-Co-Imp. Note that for Pt−Co-ySWNT-EG, the Pt precursor is reduced in the presence of Co metal particles, whereas for the Pt-SWNT-Co-Imp, a Co precursor is reduced in the presence of Pt particles.

**Catalyst Characterization.** Nitrogen physisorption of all the carbon supports was carried out on a Quantachrome Autosorb-3B static volumetric instrument. CO chemisorption was carried out on a Quantachrome Autosorb-1-C instrument. Transmission electron microscopy (TEM) images of the samples were recorded with a Philips Tecnai 12 electron microscope operated at 120 kV. The X-ray absorption spectroscopy (XAS), including both X-ray absorption near edge structure (XANES) and extended X-ray absorption fine structure (EXAFS), of the catalysts was carried out at beamline X18B at the National Synchrotron Light Source (NSLS), Brookhaven National Laboratory for both Pt $L_{III}$ edge (11564 eV) and Co K edge (7709 eV) to investigate the electronic state and coordination environment of the metals in the catalysts. The catalysts were diluted by boron nitride (from Johnson Matthey) by grinding and then pressed into a self-standing pellet. The pellet was placed into an in situ reaction cell with two beryllium windows, and then the cell was sealed with a copper gasket to prevent any possible leakage. In-situ hydrogen reduction was carried out at the beamline at 400 °C for 30 min with time-resolved XANES spectra taken, and EXAFS spectra were taken after the system was cooled to room temperature by liquid nitrogen. The XAS data was analyzed and fitted using the IFEFFIT 1.2.11 software package.[29,30] The edge jump of each sample was used to calculate the metal loading in each catalyst.

**Aqueous Phase Reforming.** The reaction activity and selectivity results for the APR reaction were tested in a fixed bed reactor described elsewhere.[8] Fifty milligrams of catalyst was loaded into a 1/4 in. stainless steel tubular reactor with quartz wool plugs and heated by an Omega ceramic fiber radiant heater. If prereduction was needed, the catalyst was reduced in hydrogen with a flow rate of 100 sccm at 400 °C for 30 min. Nitrogen was used to purge the reactor, and then the pressure was increased to the desired value (380 psig unless otherwise mentioned) and maintained using a back pressure regulator. A 10 wt % ethylene glycol aqueous solution was introduced to the reactor in an up-flow configuration via an HPLC pump, and the reactor was heated to reaction temperature over 1 h. The flow rate is 60 μL/min unless otherwise mentioned, and the reaction temperature is 225 °C unless otherwise mentioned. The gas products were swept from solution by the nitrogen carrier gas at a flow rate of 400 sccm, and the venting line was connected to a Varian CP-3800 gas chromatograph (GC) with Hayesep Q column and molecular sieve column to analyze the composition of the gaseous products. On the basis of the previous work by Dumesic and


dx.doi.org/10.1021/cs300274m | ACS Catal. 2012, 2, 1480−1486

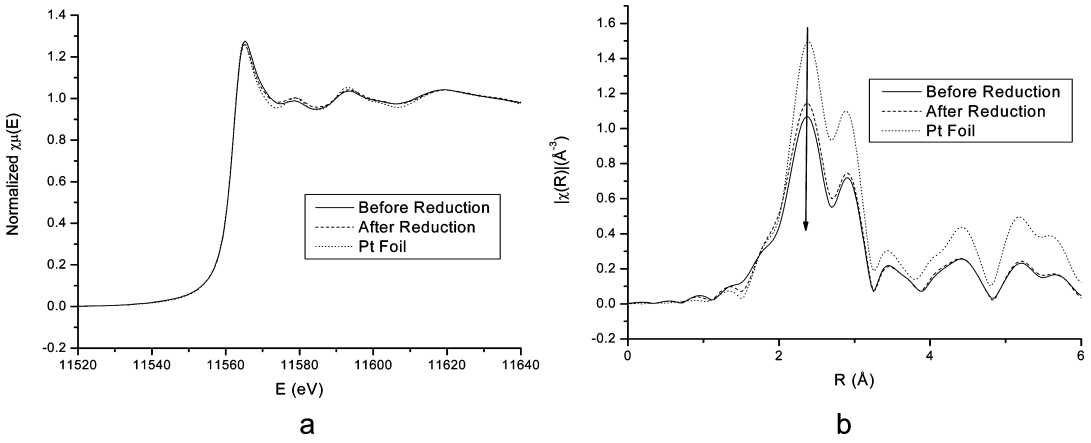


**Figure 1.** XAS results of Pt-ySWNT-EG before and after reducton: (a) XANES spectra and (b) *R* space of the EXAFS spectra.

**Table 2. The EXAFS Fitting Results of Pt Monometallic Catalysts**

| catalyst | prereduction | C.N.[a] | d*R* (Å)[b] | *R* (Å)[c] | *R* factor | $d_p$ (nm) |
|---|---|---|---|---|---|---|
| Pt-ySWNT-EG | no | 10.28 (1.29)[d] | −0.02 (0.01)[d] | 2.75[e] | 0.0061 | 2.88[e] |
| Pt-ySWNT-EG | yes | 11.08 (1.25)[d] | −0.02 (0.00)[d] | 2.75[e] | 0.0105 | 5.41[e] |
| Pt-AC | no | 9.03 (0.90)[d] | −0.02 (0.00)[d] | 2.75[e] | 0.0058 | 1.66[e] |

[a]First shell average coordination number of each absorber−scatterer pair. [b]Deviation from the interatomic distance in pure metal, which is 2.77 Å for Pt. [c]Calculated bond length from d*R*. [d]Data from the first shell coordination number fitting; data in the parentheses are uncertainties given by the IFEFFIT software. [e]Calculated using the model of refs 29 and 30. These data are not directly from the fitting; thus, uncertainty data are not included.

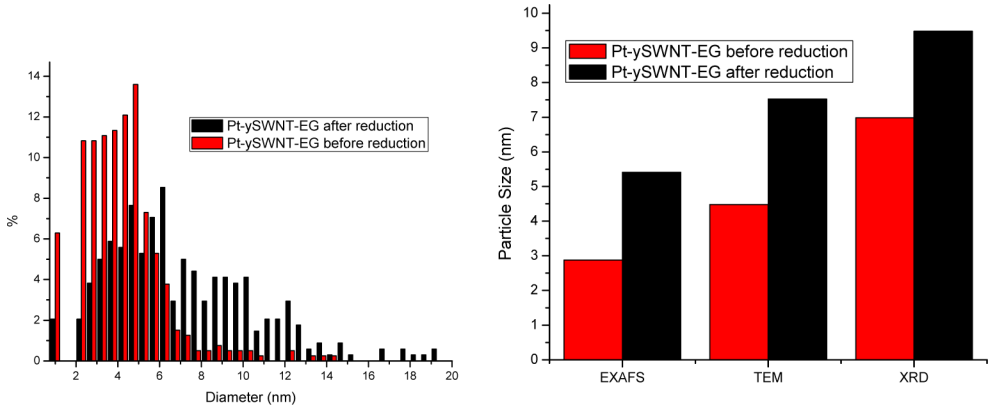


**Figure 2.** Particle size analysis of Pt-ySWNT-EG before and after reduction: (a) particle size distribution histogram from TEM and (b) comparison of particle size values from EXAFS, TEM, and XRD.

co-workers,[2−4,8] we define two kinds of reaction selectivities: hydrogen selectivity and alkane selectivity.

$$\text{hydrogen selectivity} = \left(\frac{\text{molecules } H_2 \text{ produced}}{\text{C atoms in gas phase}}\right) \times (2/5)$$

$$\text{alkane selectivity} = \frac{\text{C atoms in gaseous alkanes}}{\text{total C atoms in gas-phase product}}$$

## RESULTS AND DISCUSSION

**Carbon-Supported Pt Monometallic Catalysts for Aqueous Phase Reforming.** A screening of reaction conditions (pressure, temperature, and space velocity) was carried out, and the detailed results are discussed in the Supporting Information. The conclusion is consistent with the results of Shabaker et al.[7] on alumina-supported Pt catalyst. To compare different catalysts, the following reaction conditions were adopted: temperature 225 °C, pressure 380 psig, and WHSV 72.8 $h^{-1}$.

A comparison of the activities and selectivities on monometallic Pt catalysts supported on different carbon supports under the above-mentioned reaction conditions is listed in Table 1. It should be noted that the hydrogen selectivity and alkane selectivity do not add up to unity. This is due to the formation of liquid carbon-containing products. However, to make a fair comparison with the literature data, in Table 1, we follow the original definition of APR selectivities defined by Dumesic and co-workers.[5,7,8] A comparison between Pt-ySWNT-EG before and after hydrogen reduction clearly shows that after reduction, the activity of the catalyst is significantly decreased, which is probably due to the sintering of the Pt particles, which is also supported by the results from XAS in Figure 1. The XANES spectrum in Figure 1a shows that the Pt particles in the Pt-ySWNT-EG are at zero oxidation state even before the hydrogen reduction, and after hydrogen


dx.doi.org/10.1021/cs300274m | *ACS Catal.* 2012, 2, 1480−1486

reduction, the spectrum remains unaltered. The EXAFS, after Fourier transformation to R space, as in Figure 1b, however, shows that the amplitude of the Pt-ySWNT-EG catalyst after reduction is higher than the catalyst before reduction, indicating the sintering during the hydrogen reduction.

The first-shell average Pt−Pt coordination number can be fitted from the EXAFS data, and the corresponding Pt particle size can be further calculated using the model by Calvin and co-workers.[31,32] The average coordination number of Pt atoms in the catalyst, as well as the average particle size, were quantitatively fitted from the R space spectra, which is listed in Table 2. It is clear that after reduction, the particle size increased from less than 3 to 5.4 nm, resulting in a 40% decrease in yield and conversion. The particle size increase after reduction can also be verified by TEM and XRD results, and the results are shown in Figure 2. TEM gives larger particle size values than EXAFS. Because the EXAFS particle size results from a parameter (coordination number) that is an atom average (not a particle average) and the model is less sensitive as the coordination number approaches the bulk value of 12, it is likely that it underestimates the average particle size. Particle size values calculated from the Scherrer equation based on XRD peak broadening is larger than that from TEM because it is a volume average particle size, whereas the projected TEM particle size distribution (Figure 2a) is effectively an area average. The particle size ranking of the three methods in Figure 2b is consistent with the results by Calvin and co-workers.[32,33] Assuming the particle is spherical and the Pt atoms at the surface of the particles are in the (111) plane, we can estimate the turnover frequency by simple geometrical calculation. The turnover frequencies (TOF) of the Pt-ySWNT-EG before and after reduction are 8.5 and 9.8 $min^{-1}$ using the particle size values from EXAFS, which are the same within the uncertainty of the estimate of exposed Pt site density. It would be more accurate to calculate the TOF on the basis of the number of active sites from chemisorption measurement, but the chemisorption of Pt-ySWNT-EG was not successful, probably because during the ethylene glycol solution reduction, a chemisorbed ethylene glycol layer was retained on the surface of the particle.

The effect of different carbon supports was also studied, and the results are also shown in Table 2. Pt-AC, the catalyst with Pt nanoparticles on activated carbon, prepared by the same method as Pt-ySWNT-EG, can also catalyze APR reaction. The Pt mass time yield (mass time yield per gram of Pt) of the Pt-AC catalyst, however, is 45% lower than Pt-ySWNT-EG, although the particle size of Pt-AC is even smaller than Pt-ySWNT-EG. Thus, the ySWNT support is a better catalyst support for APR than the activated carbon support. Similarly, the same catalyst preparation method has been applied to the cSWNT support, yielding Pt-cSWNT-EG catalyst, which also gives a much lower hydrogen yield than Pt-ySWNT-EG. Thus, in the comparison among ySWNT, cSWNT, and activated carbon, ySWNT is the best catalyst support for APR. According to the previous work of Dumesic et al.,[7] for Pt/alumina catalyst, transport limitation starts to play a role when Pt loading is higher than 0.59% in a similar reactor system. We are working on different catalysts, so the conclusion is not directly transferrable, but since we are working on a much higher loading, we believe that mass transport limitation is critical under our conditions.

The nitrogen physisorption results for the three carbon supports are given in Table 3. It is straightforward that ySWNT has much higher surface area and mesopore volume than cSWNT; thus, the ySWNT-supported catalyst has a higher activity than the cSWNT-supported catalyst. On the other hand, the surface area of ySWNT is very close to the surface area of activated carbon, but the former provides much larger mesopore volume, which would facilitate for the transport of reactants and products, whereas the microporous structure of activated carbon leads to transport limitation,[34] which limits the activity of activated-carbon-supported catalysts.

**Table 3. Surface Area and Pore Volume of Different Carbon Supports**

| support | specific surface area ($m^2/g$) | mesopore volume ($cm^3/g$) |
|---|---|---|
| ySWNT | 1790 | 2.77 |
| cSWNT | 407 | 1.78 |
| activated carbon | 1800 | 0.48 |

**High-Yield Hydrogen Production from Single-Walled Carbon Nanotube-Supported Pt−Co Bimetallic Catalysts.** As we have already demonstrated, our lab-synthesized SWNT (ySWNT) is the best candidate for APR catalyst support among the three carbons studied due to its unique physical structures. Our goal in this section is to characterize the bimetallic catalysts supported on ySWNT. Three kinds of bimetallic catalysts were prepared using different procedures. The same ethylene glycol solution reduction method was adopted to decorate Pt on Co-ySWNT, yielding Pt−Co-ySWNT-EG catalyst. On the other hand, Pt and Co were sequentially impregnated onto cleaned ySWNT to obtain Pt−Co/ySWNT catalyst. A third method is to impregnate Co onto Pt-ySWNT-EG, yielding Pt-ySWNT-Co-Imp catalyst. All bimetallic catalysts were prereduced in hydrogen at 400 °C before utilization in the APR reaction.

The APR reaction activities and selectivities for the three bimetallic catalysts are listed in Table 4. Both Pt−Co-ySWNT-EG and Pt−Co/ySWNT have a significantly higher hydrogen yield than monometallic catalysts, and the selectivities, especially the alkane selectivities, have also changed significantly. The Pt-ySWNT-Co-Imp catalyst, however, shows very low activity, with an undetectable amount of hydrogen. XAS spectra, including both XANES and EXAFS, have been used to elucidate the structures of these three catalysts and to correlate the structures with the catalytic activities and selectivities.

The XANES and EXAFS spectra at both the Pt $L_{III}$ edge and Co K edge of the Pt−Co-ySWNT-EG catalyst after hydrogen prereduction are shown in Figures 3 and 4, respectively. The XANES spectra of the catalyst at both the Pt $L_{III}$ edge and Co K edge are almost identical to the Pt foil and Co foil, respectively, suggesting that both Pt and Co in the catalyst are at zero oxidation state, and there is no change of electronic structure for either Pt or Co due to alloy formation. The EXAFS results of the catalyst at both Pt $L_{III}$ edge and Co K edge also show the same shape as their bulk references, but with only lower intensities due to small particle size. Therefore, the active phases in this Pt−Co-ySWNT-EG catalyst are individual Pt and Co nanoparticles. The quantitative fitting results for the EXAFS spectra are listed in Table 5; however, as we have already demonstrated, Co-ySWNT is not an active catalyst for APR because of water oxidation of Co. The existence of Pt could retain Co in the reduced state so that both Pt and Co are active under the reaction conditions, and Co could possibly be more active than Pt. This possibility has already been demonstrated by Chen and co-workers in hydrocarbon reforming reac-


dx.doi.org/10.1021/cs300274m | ACS Catal. 2012, 2, 1480−1486

**Table 4. Aqueous Phase Reforming Activities of Pt−Co Catalysts Supported on ySWNT**

| catalyst | catalyst mass time yield[a] | Pt mass time yield[b] | % conversion[c] | % hydrogen selectivity[d] | % alkane selectivity[e] | % Pt loading[f] | % Co loading[f] |
|---|---|---|---|---|---|---|---|
| Pt−Co-ySWNT-EG | 4.56 | 58 | 42.3 | ~100 | 19.7 | 7.2 | 0.7 |
| Pt−Co/ySWNT | 2.78 | 39 | 25.6 | ~100 | 7.4 | 7.2 | 7.2 |
| Pt-ySWNT-Co-Imp | N/A[g] | N/A[g] | 1.5 | N/A[g] | 4.0 | 5.4 | 6.9 |

[a]Measured by millimoles hydrogen per gram catalyst per minute. [b]Measured by millimoles hydrogen per gram platinum in the catalyst per minute. [c]Evaluated by $CO_2$ production with respect to the ethylene glycol feed. [d]Calculated as (molecules $H_2$ produced/C atoms in gas phase)(2/5). [e]Calculated as (C atoms in gaseous alkanes)/(total C atoms in gas-phase product). [f]Calculated from the edge jump of XAS [g]The hydrogen yield for this catalyst is below the detection limit.

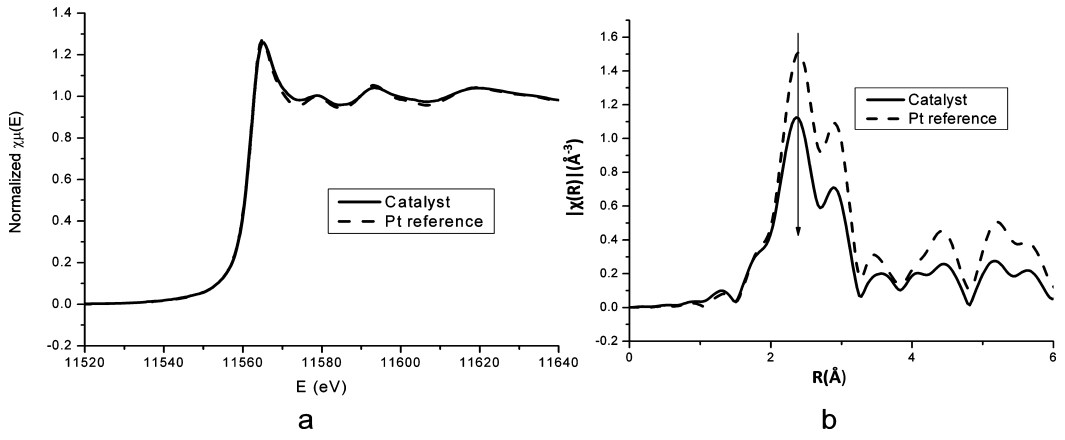


**Figure 3.** XAS results at Pt $L_{III}$ edge of Pt−Co-ySWNT-EG after reducton: (a) XANES spectra and (b) *R* space of the EXAFS spectra.

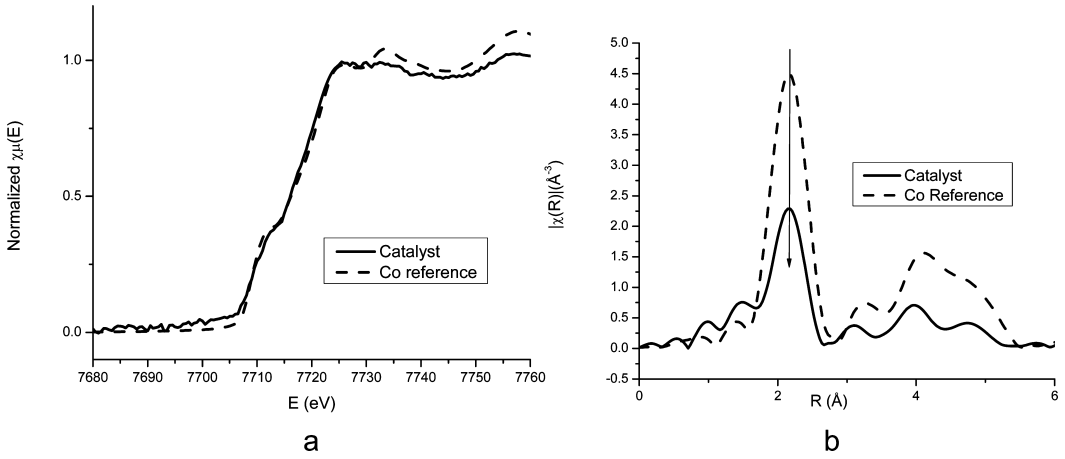


**Figure 4.** XAS results at Co K edge of Pt−Co-ySWNT-EG after reduction: (a) XANES spectra and (b) *R* space of the EXAFS spectra.

tions.[21−23] Another hint showing that Co is an active component in APR is the alkane selectivity of the Pt−Co-ySWNT-EG catalyst in APR reaction, which is significantly higher than Pt monometallic catalysts. Dumesic and co-workers have suggested that the selectivity of APR highly depends on the competition between the water−gas shift reaction (yielding $CO_2$) and the CO hydrogenation (yielding alkanes) reaction.[2,4−6] Because Co is a good CO hydrogenation catalyst, the high alkane selectivity suggests that Co may be an active component in this reaction. Recently, King et al. have also demonstrated that increasing alkane selectivity could synergistically increase the total yield of the APR reaction significantly,[13] which is consistent with our results.

The XANES and EXAFS analysis of Pt−Co/ySWNT, as well as the conclusion, are very much similar to Pt−Co/cSWNT reported in ref 11; thus, we will not repeat the details of the analyses. Readers interested in the analysis method and details may also refer to the Supporting Information as well as ref 11. In short, XANES spectra (not shown) suggested that the Pt is electron-rich and Co is electron-deficient compared with their individual foils; thus, there would be charge transfer from Co to Pt. EXAFS spectra show that Pt atoms bond mostly with Co, and Co atoms, while in excess, bond mostly with Co but also form Co−Pt bonds. The fitting results are listed in Table 5. On the basis of the Vegard's law,[35] the composition of the two components in the alloy phase can be calculated from the bond length in the alloy phase. In this catalyst, the atomic ratio between Co and Pt in the alloy phase according to Vegard's law would be 1.7; however, the bulk composition of the catalyst gives a Co/Pt ratio of 3.3, suggesting that there should be additional monometallic Co phase in the Pt−Co/ySWNT catalyst.


dx.doi.org/10.1021/cs300274m | *ACS Catal.* 2012, 2, 1480−1486

**Table 5. The EXAFS Fitting Results for Pt−Co Bimetallic Catalysts**

| catalyst | absorber | scatterer | C.N.[a] | dR (Å)[b] | R (Å)[c] | R factor |
|---|---|---|---|---|---|---|
| Pt−Co-ySWNT-EG | Pt | Pt | 10.37 (1.26)[d] | −0.02 (0.01)[d] | 2.75[e] | 0.0060 |
| | | Co | N/A[f] | N/A[f] | N/A[f] | |
| | Co | Pt | N/A[f] | N/A[f] | N/A[f] | 0.0191 |
| | | Co | 6.46 (1.70)[d] | −0.03 (0.02)[d] | 2.47[e] | |
| Pt−Co/ySWNT | Pt | Pt | N/A[f] | N/A[f] | N/A[f] | 0.0013 |
| | | Co | 5.44 (1.64)[d] | −0.17 (0.02)[d] | 2.60[e] | |
| | Co | Pt | 1.63[e] | 0.10[e] | 2.60[e] | |
| | | Co | 5.95 (0.53)[d] | 0.00 (0.00)[d] | 2.50[e] | |
| Pt-ySWNT-Co-Imp | Pt | Pt | 7.82 (1.19)[d] | −0.02 (0.01)[d] | 2.75[e] | 0.0062 |
| | | Co | 3.06 (1.14)[d] | −0.15 (0.01)[d] | 2.62[e] | |
| | Co | Pt | 0.72[e] | 0.12[e] | 2.62[e] | |
| | | O | 4.65 (3.94)[d] | 0.26 (0.03)[d] | 2.08[e] | |
| | | Co | 5.46 (3.39)[d] | 0.03 (0.05)[d] | 2.53[e] | |

[a]First shell average coordination number of each absorber−scatterer pair. [b]Deviation from the interatomic distance in pure metal, which is 2.77 Å for Pt and 2.50 Å for Co. [c]Calculated bond length from d*R*. [d]Data from the first shell coordination number fitting; data in the parentheses are uncertainties given by the IFEFFIT software. [e]Calculated from fitting constraints. These data are not directly from the fitting; thus, uncertainty data are not included. [f]Bonds are not detectable within the error range of our experiments and fittings.

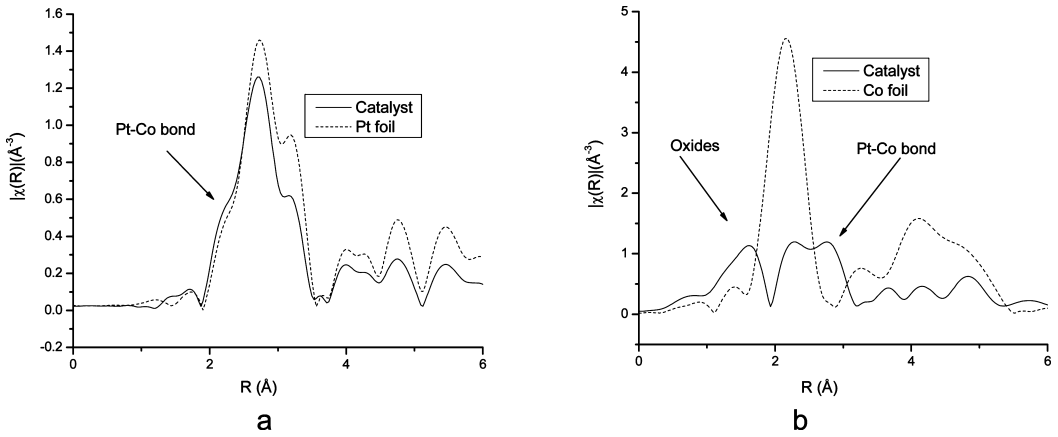


**Figure 5.** *R* space EXAFS results of Pt-ySWNT-Co-Imp catalyst at the (a) Pt $L_{III}$ edge and (b) Co K edge.

The alkane selectivity of APR over Pt−Co/ySWNT is slightly lower than the monometallic Pt catalysts, indicating that Co is not likely to be an independent active phase in this catalyst, so the additional monometallic Co phase should not be exposed to the reaction mixture. Instead, the catalyst could have a core−shell structure with a monometallic Co core and a Pt−Co alloy as the shell. The fitting results also support this core−shell model because the uncertainty of the Pt−Co bond length is larger than that of the Co−Co bond length, which is due to the surface relaxation of the former bond. The selectivity of the Pt−Co/ySWNT catalyst is in the same range as the selectivities of Pt−Co/cSWNT (reported in ref 11), indicating that this could be the intrinsic APR selectivity of the Pt−Co alloy phase.

The other bimetallic catalyst, Pt-ySWNT-Co-Imp, does not show very good activity in APR. As shown in Table 4, the hydrogen produced during the reaction could not even be detected by the TCD detector in the GC; however, a small conversion could still be measured using an FID detector, which is more sensitive than a TCD detector, to track the $CO_2$ emission during the reaction. The structural characterization by EXAFS also agrees with the low activity of the catalyst, as shown in Figure 5 and Table 5. In Figure 5a, the shoulder on the left side of the main peak of the Pt $L_{III}$ edge EXAFS spectrum of the sample indicates the existence of Pt−Co alloy bonding, but Pt−Pt bonding would still be the dominant bonding environment for Pt. On the other side, the Co K edge EXAFS spectrum in Figure 5b shows the coexistence of Co−O, Co−Co, and Co−Pt bonds. The fitting results of the EXAFS spectra are also included in Table 5. Combining the EXAFS fitting results with the low APR activity, it is likely that it is cobalt or cobalt oxide that are exposed to the reactants during reaction. During the catalyst preparation, Co precursor was impregnated on Pt metal particles. It is probable that Pt would act as the core, and Co gradually nucleates onto and is catalytically reduced on the Pt core and becomes the shell during the hydrogen reduction. Thus, the structure of this catalyst is a core−shell structure with Pt as the core and incompletely reduced Co as the shell, with Pt−Co alloy bonds forming at the core−shell interface. The large uncertainties of the fitting results of the Pt-ySWNT-Co-Imp catalyst also suggest some inhomogeneity in the sample.[36]

## CONCLUSION

SWNT-supported Pt catalysts were synthesized and tested for APR reactivity. The optimal reaction conditions are obtained, and the catalyst showed higher hydrogen productivity than traditional catalysts supported on oxides. EXAFS results indicate that Pt(0) is the effective catalyst in this reaction, and smaller Pt nanoparticles give better activity. Moreover, ySWNT-supported Pt catalyst shows better performance than

activated carbon and commercial SWNT-supported Pt catalysts, demonstrating the advantage of SWNT supports made in our laboratory, which have a combination of high surface area and large mesopore volume relative to the other two carbons.

The introduction of Co to Pt catalysts enhances the catalyst performance. Two kinds of bimetallic catalysts were found to have higher hydrogen yield than Pt monometallic catalysts operated under the same reaction conditions, and structural studies show that the two bimetallic catalysts promote the APR reaction in two different ways: In Pt−Co-ySWNT-EG catalyst, individual Pt and Co particles are both active phases in the reaction, and the synergistic interaction between the two metals guarantees that Co particles will be in a reduced state, maintaining their high activity. On the other hand, the Pt−Co/ySWNT catalyst has a core−shell structure with Co as the core and Pt−Co alloy as the shell, and the alloy phase is the active phase during the APR reaction. The difference in their APR selectivities of the two bimetallic catalysts also verifies the structural models proposed here.

## ■ ASSOCIATED CONTENT

### Supporting Information

Activities of Co-ySWNT catalyst, screening of reaction conditions using Pt-ySWNT catalyst, detailed EXAFS analysis for Pt−Co/ySWNT. This material is available free of charge via the Internet at http://pubs.acs.org.

## ■ AUTHOR INFORMATION


### Corresponding Author

*(X.W.) Phone: 1-732-205-6080. E-mail: xiaoming.wang@basf.com. (G.L.H.) Phone: 1-203-432-4378. E-mail: gary.haller@yale.edu.

### Present Addresses

[†]BASF Corporation, 25 Middlesex/Essex Turnpike, Iselin, NJ 08830, USA

[‡]The Boston Consulting Group, 1 Prospect St., Summit, NJ 07901, USA

[§]Institute of Chemical and Engineering Sciences, A-STAR, 1 Pesek Road, Jurong Island, Singapore 627833.


### Notes

The authors declare no competing financial interest.

## ■ ACKNOWLEDGMENTS

The authors are grateful to the DOE, Office of Basic Energy Sciences, Grant FG02-05ER15732, and AFOSR MURI Grant FA9550-08-0309 for financial support. We also acknowledge NSLS at Brookhaven National Laboratory for X-ray beamtime at beamlines X18B and X23A2, and thank Drs. Nebojsa Marinkovic and Bruce Ravel for the on-site technical support.

## ■ REFERENCES


(1) Nemanich, G.; Katsaros, A.; Niedzwiecki, A.; Davis, J. M.; Balog, F.; Serfass, J.; Ogden, J. *National Hydrogen Energy Roadmap; Energy*; U.S. DOE: Washington, DC, 2002.

(2) Cortright, R. D.; Davda, R. R.; Dumesic, J. A. *Nature* **2002**, *418*, 964.

(3) Davda, R. R.; Dumesic, J. A. *Chem. Commun.* **2004**, 36.

(4) Huber, G. W.; Dumesic, J. A. *Catal. Today* **2006**, *111*, 119.

(5) Shabaker, J. W.; Huber, G. W.; Davda, R. R.; Cortright, R. D.; Dumesic, J. A. *Catal. Lett.* **2003**, *88*, 1.

(6) Davda, R. R.; Shabaker, J. W.; Huber, G. W.; Cortright, R. D.; Dumesic, J. A. *Appl. Catal., B* **2005**, *56*, 171.

(7) Shabaker, J. W.; Davda, R. R.; Huber, G. W.; Cortright, R. D.; Dumesic, J. A. *J. Catal.* **2003**, *215*, 344.

(8) Huber, G. W.; Shabaker, J. W.; Evans, S. T.; Dumesic, J. A. *Appl. Catal., B* **2006**, *62*, 226.

(9) Wang, X. M.; Li, N.; Pfefferle, L. D.; Haller, G. L. *Catal. Today* **2009**, *146*, 160.

(10) Wang, X. M.; Li, N.; Webb, J. A.; Pfefferle, L. D.; Haller, G. L. *Appl. Catal., B* **2010**, *101*, 21.

(11) Wang, X. M.; Li, N.; Pfefferle, L. D.; Haller, G. L. *J. Phys. Chem. C* **2010**, *114*, 16996.

(12) Kim, T. W.; Kim, H. D.; Jeong, K. E.; Chae, H. J.; Jeong, S. Y.; Lee, C. H.; Kim, C. U. *Green Chem.* **2011**, *13*, 1718.

(13) King, D. L.; Zhang, L. A.; Xia, G.; Karim, A. M.; Heldebrant, D. J.; Wang, X. Q.; Peterson, T.; Wang, Y. *Appl. Catal., B* **2010**, *99*, 206.

(14) Sinfelt, J. H. *Bimetallic Catalysts: Discoveries, Concepts, And Applications*; Wiley: New York, 1983.

(15) Freund, A.; Lang, J.; Lehmann, T.; Starz, K. A. *Catal. Today* **1996**, *27*, 279.

(16) Kiros, Y. *J. Electrochem. Soc.* **1996**, *143*, 2152.

(17) Paulus, U. A.; Wokaun, A.; Scherer, G. G.; Schmidt, T. J.; Stamenkovic, V.; Radmilovic, V.; Markovic, N. M.; Ross, P. N. *J. Phys. Chem. B* **2002**, *106*, 4181.

(18) Salgado, J. R. C.; Antolini, E.; Gonzalez, E. R. *J. Power Sources* **2004**, *138*, 56.

(19) Travitsky, N.; Ripenbein, T.; Golodnitsky, D.; Rosenberg, Y.; Burshtein, L.; Peled, E. *J. Power Sources* **2006**, *161*, 782.

(20) Saejeng, Y.; Tantavichet, N. *J. Appl. Electrochem.* **2009**, *39*, 123.

(21) Lu, S. L.; Lonergan, W. W.; Bosco, J. P.; Wang, S. R.; Zhu, Y. X.; Xie, Y. C.; Chen, J. G. *J. Catal.* **2008**, *259*, 260.

(22) Lu, S. L.; Menning, C. A.; Zhu, Y. X.; Chen, J. G. *ChemPhysChem* **2009**, *10*, 1763.

(23) Lu, S. L.; Lonergan, W. W.; Zhu, Y. X.; Xie, Y. C.; Chen, J. G. G. *Appl. Catal., B* **2009**, *91*, 610.

(24) Li, N.; Wang, X. M.; Ren, F.; Haller, G. L.; Pfefferle, L. D. *J. Phys. Chem. C* **2009**, *113*, 10070.

(25) Lim, S.; Li, N.; Fang, F.; Pinault, M.; Zoican, C.; Wang, C.; Fadel, T.; Pfefferle, L. D.; Haller, G. L. *J. Phys. Chem. C* **2008**, *112*, 12442.

(26) Chen, Y.; Wei, L.; Wang, B.; Lim, S. Y.; Ciuparu, D.; Zheng, M.; Chen, J.; Zoican, C.; Yang, Y. H.; Haller, G. L.; Pfefferle, L. D. *ACS Nano* **2007**, *1*, 327.

(27) Koningsberger, D. C.; Prins, R. *X-ray Absorption: Principles, Applications, Techniques of EXAFS, SEXAFS, and XANES*; Wiley: New York, 1988.

(28) Lordi, V.; Yao, N.; Wei, J. *Chem. Mater.* **2001**, *13*, 733.

(29) Newville, M. *J. Synchrotron Radiat.* **2001**, *8*, 322.

(30) Ravel, B.; Newville, M. *J. Synchrotron Radiat.* **2005**, *12*, 537.

(31) Calvin, S.; Miller, M. M.; Goswami, R.; Cheng, S. F.; Mulvaney, S. P.; Whitman, L. J.; Harris, V. G. *J. Appl. Phys.* **2003**, *94*, 778.

(32) Calvin, S.; Luo, S. X.; Caragianis-Broadbridge, C.; McGuinness, J. K.; Anderson, E.; Lehman, A.; Wee, K. H.; Morrison, S. A.; Kurihara, L. K. *Appl. Phys. Lett.* **2005**, *87*.

(33) Calvin, S.; Riedel, C. J.; Carpenter, E. E.; Morrison, S. A.; Stroud, R. M.; Harris, V. G. *Phys. Scr.* **2005**, *T115*, 744.

(34) Liang, Y. R.; Liang, F. X.; Wu, D. C.; Li, Z. H.; Xu, F.; Fu, R. W. *Phys. Chem. Chem. Phys.* **2011**, *13*, 8852.

(35) Vegard, L. *Z. Phys.* **1921**, *5*, 17.

(36) Moonen, J.; Slot, J.; Lefferts, L.; Bazin, D.; Dexpert, H. *Phys. B: Condens. Matter* **1995**, *208*, 689.